

## 5. Materials and Methods

### 5.1 Material

Selected quinones (Table 5.1), fluorenones and reagents for the preparation of buffers were purchased from Aldrich. Perdeuterated quinones: d<sub>6</sub>-1,4-naphthoquinone, d<sub>8</sub>-2-methyl-1,4-naphthoquinone, d<sub>10</sub>-2-ethyl-1,4-naphthoquinone, as well as selectively labeled d<sub>2</sub>-2-ethyl-1,4-naphthoquinone, 2-methyl-4-<sup>13</sup>C-1,4-naphthoquinone, 2-methyl-<sup>13</sup>C-1,4-naphthoquinone were synthesized (see Figure 5.1).

All EPR samples contained 1 mM sodium ascorbate and 50 μM phenazine methosulfate as external redox agents and were frozen in the dark for the low temperature experiments.

### Buffers

1. 50 mM Tris, pH=8.3 with 0.2% Triton X100
2. 50 mM Tris, pH=8.3 with 0.02% n-dodecyl-β-D-maltoside (β-DM)
3. 50 mM MES, pH=5.4 with 0.2% Triton X100

### 5.2 Quinones

2-ethyl-1,4-naphthoquinone-d<sub>10</sub> was prepared by oxidation of 2-ethylnaphthalene-d<sub>12</sub> with CrO<sub>3</sub> in acetic acid. The perdeuteration of 2-ethylnaphthalene was accomplished by catalytic exchange with D<sub>2</sub>O in a high pressure vessel (6 days at 280 °C) with platinum on carbon as the catalyst. Three subsequent exchange reactions resulted in 2-ethylnaphthalene-d<sub>12</sub> with D=98% as confirmed by NMR and mass spectroscopy. 2-ethyl-α,α-d<sub>2</sub>-1,4-naphthalene was obtained by reduction of 2-methylnaphthylketone with AlCl<sub>3</sub>/LiAlD<sub>4</sub> 1:1 under reflux in ether. The isolated and

distilled product was oxidized to 2-ethyl- $\alpha,\alpha$ -d<sub>2</sub>-1,4-naphthoquinone with Cr(VI) oxide as described above. D=98%.

The starting compound for the synthesis of 2-methyl-4-<sup>13</sup>C-naphthoquinone was 2-methylcinnamic acid, prepared according to [58] by a modified Perkin reaction from benzaldehyde and propionic anhydride, was reduced to 2-methylcinnamylalcohol with LiAlH<sub>4</sub> in ether. Catalytic hydrogenation to 2-benzyl-1-propanol was accomplished with fresh reduced Adam's catalyst PtO<sub>2</sub> in methanol. Conversion to the 2-benzylpropylbromide with SOCl<sub>2</sub> was followed by carboxylation of the corresponding Grignard reagent with <sup>13</sup>CO<sub>2</sub> (from Ba<sup>13</sup>CO<sub>3</sub>, -30°C, ether) to 3-benzylbutyric acid-1-<sup>13</sup>C. Cyclisation to 2-methyl-4-<sup>13</sup>C-4-tetralone was made via the acidchloride of 3-benzylbutyric-acid-1-<sup>13</sup>C (SOCl<sub>2</sub>, RT) with polyphosphoric acid as described for tetralone [59]. Clemmensen reduction of 2-methyl-4-<sup>13</sup>C-4-tetralone resulted in 2-methyl-4-<sup>13</sup>C-tetraline, followed by dehydrogenation with palladium on charcoal to 2-methyl-4-<sup>13</sup>C-naphthalene. Oxidation with CrO<sub>3</sub> in the usual way yielded 2-methyl-4-<sup>13</sup>C-1,4-naphthoquinone.

For synthesis of 2-<sup>13</sup>C-methyl-1,4-naphthoquinone the 2-naphthoic-acid-carboxyl-<sup>13</sup>C was prepared by carboxylation with <sup>13</sup>CO<sub>2</sub> of 2-naphthylmagnesiumbromide. The naphthoic acid was reduced by LiAlH<sub>4</sub> to 2-naphthalenemethanol-<sup>13</sup>C followed by conversion to the bromide. Dehalogenation with LiAlH<sub>4</sub> resulted in 2-<sup>13</sup>C-methylnaphthalene. Oxidation with CrO<sub>3</sub> yielded the 2-<sup>13</sup>C-methyl-1,4-naphthoquinone.

The precise labeling of the 2-methyl-1,4-naphthoquinones, the percentage of isotope as well as the chemical purity was checked by <sup>13</sup>C and <sup>1</sup>H-NMR and mass-spectrometry and found better than 99 %.

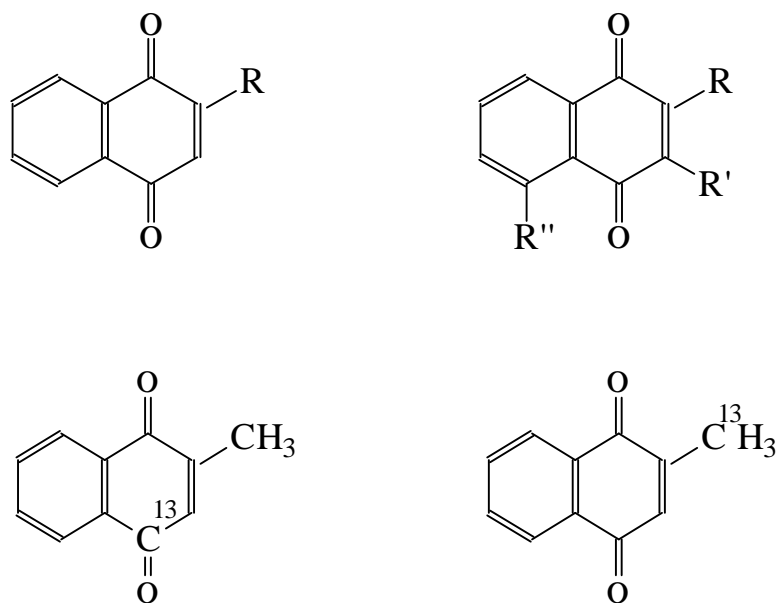
### 5.3 Preparation of Photosystem I samples with artificial quinines

#### 5.3.1 Quinone reconstitution into PS I after organic solvent extraction

PS I isolated from *Synechocystis* PCC 6803 was prepared by the method of Biggins and Mathis [60]. The isolated PS I was lyophilized and the native phylloquinone was removed by solvent extraction as described in [60, 46] using hexane (99%, Aldrich) containing 0.3% methanol (Caledon). The extraction of the phylloquinone was monitored using a modified Bruker ESP 200 X-band spectrometer (described below 5.4) by measuring the disappearance of the spin polarized EPR signal due to  $P_{700}^+A_1^-$  and accompanying appearance of  ${}^3P_{700}$  formed by recombination from  $P_{700}^+A_0^-$ . The loss of other pigments was monitored using the visible absorption spectrum of the supernatant recorded with a Unicam UV/Vis spectrometer. Samples for EPR analysis were prepared by suspending 15 mg of extracted PS I in 150  $\mu$ l of buffer containing 50 mM Tricine, 10% glycerol and 0.2% Triton X-100. A homogenizer was used to ensure complete resuspension. A series of quinones were introduced into the  $A_1$  binding site by incubating the extracted PS I with an excess of quinone. The quinone (~150 mM) was prepared in either ethanol, 1-propanol or dimethylsulfoxide solution and added to the resuspended PS I sample to give a 1000:1 molar ratio of quinone to PS I. The samples were then incubated in the dark at 4°C, with incubation times ranging from 30 minutes to 3 hours. The incorporation of quinone into the  $A_1$  site was monitored by observing the appearance of a spin polarized EPR spectrum due to  $P_{700}^+NQ^-$  accompanied by the disappearance of the  ${}^3P_{700}$  spectrum. Control experiments using blanks of the three solvents containing no quinone were also performed and no change in the transient EPR spectra was observed. For the EPR experiments 1 mM sodium ascorbate and 50  $\mu$ M phenazine methosulfate were added as external redox agents and the samples were frozen in the dark.

### 5.3.2 Substitution of plastoquinone –9 in the PS I trimers isolated from *menB* mutant

Different quinones as well as fluorenones (Tables 5.1, 5.2) were used for the plastoquinone-9 substitution in the A<sub>1</sub> site of PSI from *menB* mutant. The 100 times mol. excess of quinone (10µl of 0.034 M solution of quinone in ethanol) was added to the 150 µl PS I particles suspension in the 50 mM Tris buffer pH=8.3 (0.2% triton X100). The reaction was performed at room temperature (2-4 h) under intensive stirring. After the reaction the PS I particles were washed 2 times with 150 µl of buffer solution in order to remove any excess of quinones. This operation was done in the concentrator vessels. The solvent was removed by centrifugation. The final volume of sample was 150µl. The control of substitution of PQ-9 was done by TR-EPR spectroscopy at 80K.

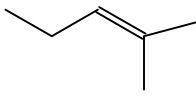
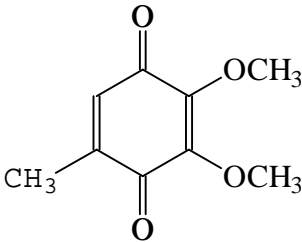
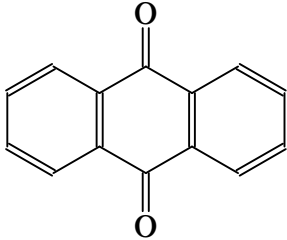
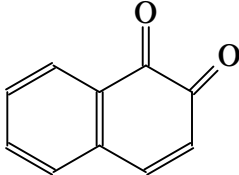
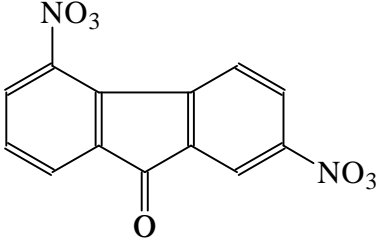


**Figure 5.1** Molecular structure of 1,4-naphthoquinone derivatives used for the incorporation into the A<sub>1</sub> site of PS I. For the radical –R structure see Table 5.1. For the radicals –R, –R' and –R'' structure see Table 5.2

Table 5.1 Structure of quinones used for the incorporation into the A<sub>1</sub> site of PS I (position of the radical –R in the 1,4-naphthoquinone ring shown on the Figure 5.1), experimental conditions and substitution result.

-R	Buffer	pH	Time	Quinone excess	Substitution
-H	50 mM Tris +0.2% Triton	8.3	2h	100 molar %	Full
-CH <sub>3</sub> , -CD <sub>3</sub>					
-CH <sub>2</sub> -CH <sub>3</sub>					
-CD <sub>2</sub> -CH <sub>3</sub>					
-CD <sub>2</sub> -CD <sub>3</sub>					
Butyl-					

Table 5.2 Structure of quinones used for the incorporation into the A<sub>1</sub> site of PS I (position of the radical -R, -R' and -R'' in the 1,4-naphthoquinone ring shown on the Figure 5.1), experimental conditions and substitution result.

R	R'	R''	Buffer	pH	Time	Quinone excess	Substitution
-NH <sub>2</sub>	-H	-H	50 mM Tris +0.2% Triton	8.3	4h	100 molar %	Full
-OH	-H	-H	50 mM MES +0.2% Triton	5.4	2h		Partial
-CH <sub>3</sub>	-H	-OH			4h		Full
-OH		-H			4h		Full
					50 mM Tris +0.2% Triton		8.3
			4h	Partial			
			2h	No			
			4h	No			

#### 5.4 Time resolved EPR spectroscopy

Time resolved EPR spectroscopy has been widely used to gain information on transient intermediates, which occur in light-induced photoreactions. As mentioned previously, a useful feature of light-generated radical pairs in photosynthetic reaction centers is the occurrence of electron spin polarisation. Besides a crucial signal enhancement, the observable polarisation pattern carries important information on the spin system, in particular associated with the geometrical arrangement of the cofactors involved, reaction pathway and kinetics.

The time resolved EPR (TR-EPR) spectroscopy was used in this work to obtain information on the radical pair state. It was performed at different frequency bands (X, Q, W) using a narrow excitation bandwidth together with direct detection of the EPR signal. Transient EPR experiments are based on conventional cw-EPR spectroscopy with continuous irradiation of the spin system applying low-power microwave irradiation. The radical pair state is usually generated by a laser flash at some instant of time and the transient EPR signal at a fixed magnetic field is detected as function of time.

The experimental spectrum is depicted in the Figure 5.2 (top). An advantage of the use of a relative weak microwave field is the possibility of detecting the signal without deadtime, since there is no need to protect the detector from high-power microwave. Most of the transient EPR spectra described in this thesis have been recorded in the direct detection mode, providing fast time resolution. In this mode, the signal is observed at the output of the pre-amplifier without field modulation or lock-in technique. Note that the EPR spectra taken in this way do not appear in the conventional first-derivative form but show absorption (A) or emission (E). All TR-EPR spectra presented in this thesis have on y-axis imaginary part of magnetic susceptibility  $\chi''$  in arbitrary units (a.u.) and on x-axis magnetic field in mT or time.

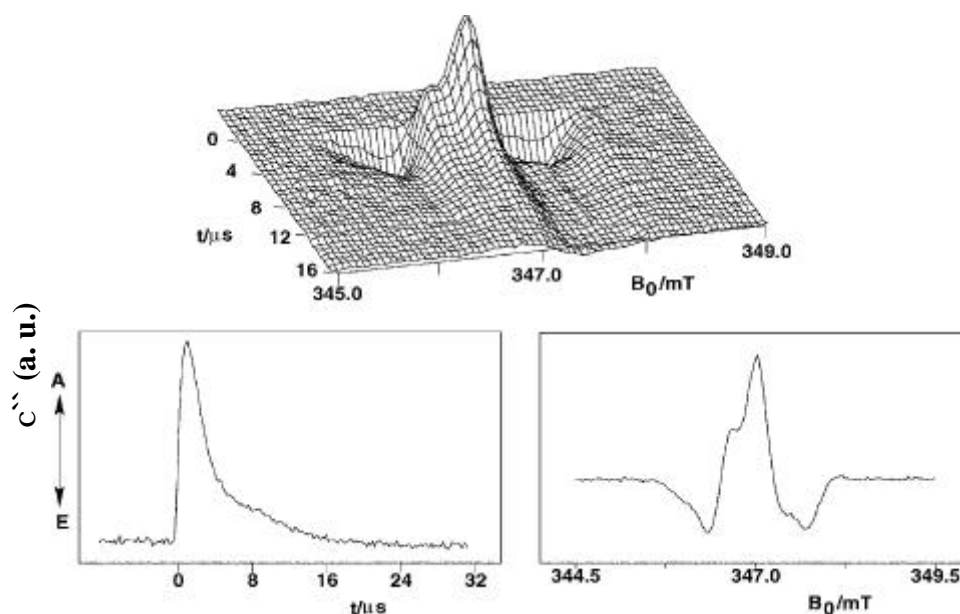


**Figure 5.2** Transient EPR of the radical pair state  $P_{700}^+A_1^-$  in PS I. Top: Two dimensional representation of the time and magnetic field dependence of the TR-EPR signal. Bottom (left): Time development of the EPR signal. Bottom (right): TR-EPR spectrum extracted from the 2D-data set by integration of the time signal between 1 and 2  $\mu\text{s}$  after the laser flash.

The need of broad band amplification of the signal in order to achieve high time-resolution results in a reduced sensitivity, i.e. a lower signal-to-noise ratio. However, as mentioned above, one can benefit from electron spin polarisation which yields much stronger signals than expected for systems in thermal equilibrium due to selective population of energy levels far from Boltzmann distribution.

The time-resolved EPR experiments at X-band (9 GHz) were performed on a set up as described [61] with a ER 4118 X-MD-5W1 dielectric ring probehead and a helium cryostat (Oxford CF935). The loaded  $Q$ -value for this dielectric ring resonator was about  $Q=3000$ , equivalent to a rise time of  $t_r = Q/(2p \cdot n_{mw}) \approx 50$  ns. Q-band (35 GHz) transient EPR spectra were measured in a set up as described earlier [62], except that a Bruker ER 056 QMV microwave bridge equipped with a home built cylindrical resonator and an Oxford CF935 liquid helium cryostat was used. The light source for the experiments was a



Q-switched and frequency-doubled Nd-YAG laser (Spectra Physics GCR 130) working at  $\lambda=532$  nm with a pulses width of 8 ns (full width at half height) and a repetition rate of 10 Hz. The excitation energy was approximately  $3 \text{ mJ/cm}^2$  at the surface of EPR tube.

The transient EPR signals were recorded using a LeCroy 9450A 350MHz digital oscilloscope, equipped with the WP01 waveform package. The oscilloscope uses a trigger pulse from a photodiode placed close to the entrance for the laser light in the resonator. A complete data set is a series of transient signals measured at equidistant magnetic field points covering the total spectral width. In Figure 5.2 (top), an example of the time and magnetic field dependence of the transient EPR signal is shown in a two-dimensional plot. The time dependence of the magnetisation is shown in Figure 5.2 bottom (left) at the field position with the absorption signal at maximum. The Figure 5.2 bottom (right) shows the transient EPR spectrum obtained by digital boxcar integration of the time-signal within a specified integration gate  $[t_1, t_2]$ , according to relation:

$$I(B_0) = \frac{\int_{t_1}^{t_2} I(t, B_0) dt}{t_2 - t_1} - \frac{\int_{t_1'}^{t_2'} I(t, B_0) dt}{t_2' - t_1'}$$

For the base line correction an average of off-resonance transients was subtracted from each transient within the data set, thus eliminating the laser background (shifts due to photo-induced effects inside the resonator).

### 5.5 Pulsed ENDOR studies of the $P_{700}^+A_1^-$ state

The ENDOR technique can be used to determine hfs with high precision even they are not resolved in the TR-EPR spectra. In this technique, the nuclear transitions are detected by monitoring changes in the amplitude of the EPR line. In the ENDOR spectra

sets of equivalent nuclei show two lines symmetrically spaced about the nuclear Larmor frequency  $\nu_n$

$$\nu_{\text{ENDOR}}^{\pm} = |\nu_n \pm A/2|,$$

where  $A$  is the isotropic hfs. For this work it was necessary to perform pulsed, time resolved ENDOR experiments. Measurements have been done directly with the short-lived photoinduced radical pair state  $P_{700}^+A_1^-$ . The peculiarity of such an experiment is that the unpaired electron spins are located on the two chemically different radical species. Therefore, ENDOR spectra of  $P_{700}^+A_1^-$  represent a superposition of the spectra from  $P_{700}^+$  and  $A_1^-$ . An additional feature is the emissive and absorptive components in the spectra, which arise because of the spin polarisation of the radical pair state. The overlapping of different emissive and absorptive peaks lead in general to an asymmetry of the spectra relative to the Larmor frequency that might be confusing in comparison to stable radical ENDOR spectra which are usually symmetric. Nearly symmetric pulsed ENDOR spectra can be recorded at the field position slightly shifted up field from the E/A zero crossing point of the TR-EPR spectra. At this field position the ENDOR spectra look the most symmetric. Pulsed ENDOR studies of the  $P_{700}^+Q^-$  radical pair were performed on Bruker ESP 380E X-band FT-EPR spectrometer using a ESP360D-P ENDOR accessory, an ER4118X-MD-5W1-EN ENDOR resonator and an ENI A500 radiofrequency amplifier. The Davies-ENDOR pulse sequence ( $\pi$ (microwave) -  $\pi$ (radio frequency) -  $\pi/2$ (microwave) -  $\pi$ (microwave) – echo) was used, with pulse lengths of 128 ns for the two microwave  $\pi$  pulses and 64 ns for a microwave  $\pi/2$  pulse and 8  $\mu$ s for the radio frequency  $\pi$  pulse. The delay time between the laser flash and the first microwave pulse was 800 ns. The ENDOR experiments were carried out at 80 K.

The light source for the experiments was a Q-switched and frequency-doubled Nd-YAG laser (Spectra Physics GCR 130) operating at  $\lambda = 532$  nm wavelength of 532 nm with a pulse width of 8 ns (full width at half height) and a repetition rate of 10 Hz.

### 5.6 Electron transfer kinetics from phylloquinone to iron-sulphur clusters [27].

The TR-EPR measurements at high temperature (room temperature and 260K) give access to the electron transfer kinetic from PhQ molecule to iron-sulphur clusters. At these high temperatures the kinetics of electron transfer are faster than the relaxation of the spin polarisation in TR-EPR spectra. This means that in the TR-EPR dataset two sequential radical pairs can be observed: an early (E/A/E) signal attributed to  $P_{700}^+A_1^-$  radical pair and a late mainly (E) signal due to  $P_{700}^+(FeS)^-$ . The transition from the early signal to the late signal is due to electron transfer. Global spectral analysis allows the rate constants of the various processes which influence the EPR signals as well as the kinetically separated spin-polarized EPR spectra of the involved charge separated states to be extracted from the complete time-field data set.

In general, the transient EPR signal of a sample with several consecutive light-induced paramagnetic species is a function of the magnetic field strength,  $B_0$  and the time  $t$  and it can be described by a sum of signal contributions:

$$S(t, B_0) = \sum_i S_i(t, B_0)$$

The signal of given species  $S_i(B_0, t)$  depends on the evolution with time of its concentration and spin polarisation. For the reaction  $A^\bullet \rightarrow B^\bullet$ , is modeled as:

$$S_A(t, B_0) = \mathbf{a}(B_0)e^{-(k+w_A)t}$$

$$S_B(t, B_0) = \mathbf{b}(B_0) \frac{k}{k + w_A - w_B} \left\{ e^{-w_B t} - e^{-(k+w_A)t} \right\}$$

where  $k$  is the first-order reaction rate constant,  $\omega_A$  and  $\omega_B$  are the decay rates of the spin polarisation in species  $A^\bullet$  and  $B^\bullet$ , respectively, and  $\alpha(B0)$  and  $\beta(B0)$  are their spin-polarized EPR spectra in the absence of relaxation. The decay of spin polarised signal is given by the spin-lattice relaxation rate in the limit-zero microwave power [63]. For finite values of the microwave power,  $\omega_A$  and  $\omega_B$  are effective relaxation rates which will be smaller than the true spin-lattice relaxation rates. In the equations no assumptions have been made concerning the relative magnitudes of  $k$ ,  $\omega_A$  and  $\omega_B$ . If these rate constants are sufficiently smaller than the inverse of the spectrometer response time, then the equations will satisfactorily describe the observed signal dependence. In the case of PS I  $k^{-1}=200$  ns whereas the response function is a simple exponential with an inverse rate constant of  $\approx 50$  ns. Thus, this condition is not well fulfilled and the response of spectrometer should be taken into account. This can be done by calculating the convolution integral of the response function and the above EPR signal dependence.

### *5.7 Room Temperature Transient EPR measurements*

Room temperature X-band experiments were performed using a modified Bruker ESP 200 spectrometer equipped with a home-built, broadband amplifier (bandwidth  $>500$  MHz). A flat cell and a rectangular resonator were used and the samples were illuminated using a Q-switched, frequency- doubled Continuum Surelite Nd-YAG laser at 532 nm with a repetition rate of 10 Hz. 1 mM NaAsc and 50  $\mu$ M PMS phenazine methosulfate were added to mediate cyclic electron transfer.

### *5.8 Selective point mutagenesis in the PS I protein complex.*

Point mutants of the PS I protein complex were prepared by Wu Xu in the group of P. Chitnis (Iowa State University). Biosynthetic pathway mutants were prepared by Gaozhong Shen in the D.A. Bryant's and J.H. Golbeck's groups (Pennsylvania State

University). The point mutants that were investigated are listed in the Table 5.3. Specific amino acids in the neighbourhood of the acceptors  $A_0$ ,  $A_1$  and  $F_x$  binding sites were targeted in either A or B branches of electron transfer in PS I.

The mutant preparation is the multi step state-of-art procedure (for experimental details see [64]). Here only a short outline will be provided. For the preparation of the mutants, genes coding the PsaA or PsaB subunits were isolated from the cyanobacterial DNA. After that each gene was incorporated into the plasmid modified by adding the special DNA sequence that is responsible for conferring antibiotic resistance of the cells, and *Escherichia coli* (*E. coli*) cells were transformed with it. The plasmid was amplified in *E. coli* cells and then separated. The point mutation was done by cutting the specific restriction site and introducing synthetic oligonucleotide carrying desired mutation. The mutated plasmid was amplified in the *Escherichia coli* (*E. coli*) cells and separated. Cyanobacteria were then transformed with the plasmid carrying the mutant gene.

The mutants were segregated by growing cyanobacteria in media containing antibiotic lethal to the cells that lack the mutation. The mutation was confirmed by DNA sequencing. Physiological characterization was done by growing cells at different light intensities under photomixotrophic or photoautotrophic growth conditions, *i.e.* with or without glucose. PS I complexes were isolated from the mutant strains of cyanobacterial cells and purified according to procedure described before [65]. All mutations were confirmed by DNA sequencing.

Activity of the PS I complexes from the mutants was determined by light-driven PS I-mediated electron transport from 3,6 diaminodurene to methyl viologen using a Clark type oxygen electrode and with a  $NADP^+$  photoreduction assay using cytochrome  $c_6$  and ferredoxin as electron donor and acceptor respectively [65].

Table 5.3. Point mutants of photosystem I that have been studied by EPR.

Cofactor binding site	PsaA	PsaB
A <sub>0</sub> , chlorophyll	Met→Leu	Met→Leu
	M688L	M668L
A <sub>1</sub> , Phylloquinone	Trp→Phe	Trp→Phe
	W697F	W677F
	Ser→Cys	Ser→Cys
	S692C	S672C
	Phe→Tyr	Phe→Tyr
	F689Y	F669Y
F <sub>x</sub> , [4Fe-4S] cluster	Arg→Ala	Arg→Ala
	R694A	R674A